Engineering Structures 198 (2019) 109535

Contents lists available at ScienceDirect

Engineering Structures

journal homepage: www.elsevier.com/locate/engstruct

Prediction of bond performance of tension lap splices using artificial neural networks

Hyeon-Jong Hwang[a], Jang-Woon Baek[b], Jae-Yo Kim[c], Chang-Soo Kim[d,*]

[a] College of Civil Engineering at Hunan University and Key Laboratory for Damage Diagnosis of Engineering Structures of Hunan Province, Changsha, Hunan, China
[b] Department of Civil Engineering and Environmental Sciences at Korea Military Academy, Seoul, South Korea
[c] Department of Architectural Engineering at Kwangwoon University, Seoul, South Korea
[d] School of Architecture at Seoul National University of Science and Technology, Seoul, South Korea

ARTICLE INFO

Keywords:
Artificial neural networks
Bond strength
Development length
Lap splice length
Splice test
Non-uniform bond stress distribution

ABSTRACT

Recently, machine learning has been widely used in civil engineering, because better design can be achieved using the advanced computer intelligence and test results. In the present study, to improve design reliability and to extend design application range for the development and lap splice lengths, an artificial neural network model (ANN) was presented using 1008 existing experimental studies for splice tests. Although some of the test parameters are out of the limitations of design codes, all test results were used for the ANN to extend design application range considering present-day construction materials and practices. From a parametric study with the ANN, the effect of design variables was investigated, and predictions by the ANN were compared with existing design equations. Finally, based on the parametric study result, modifications were proposed for existing design equations to consider the effect of non-uniform bond stress distribution and the effect of cover concrete and transverse bars, as well as to extend design application range. Comparisons showed that the modifications improved the accuracy of the design methods. The high accuracy to the large number of existing test results confirms that the modifications based on the ANN can improve design reliability and also can extend design application range for the development and lap splice lengths.

1. Introduction

In reinforced concrete (RC) structures, the stress of reinforcing bars embedded in concrete is transferred to concrete by bond between the steel and concrete. Thus, to develop the desired strength of reinforcing bars, sufficient development and lap splice lengths should be provided. Development length represents the bonded length of a reinforcing bar that is not spliced with another reinforcing bar, while lap splice length represents the bonded length of reinforcing bars that are lapped spliced.

Current design codes such as ACI 318-14 [1], ACI 408R-03 [2], Eurocode 2 [3], and fib Model Code 2010 [4] specify requirements for the development and lap splice lengths based on test results with the splice specimen configuration [2] (hereafter, splice tests). However, the development length concept in the design codes is based on the attainable average bond stress over the embedment length [1]. To achieve more accurate and economical design, significant efforts have been made. On the basis of existing splice test results, Orangun et al. [5] performed nonlinear regression analysis, in which the concrete strength, bar diameter, clear bar spacing, cover concrete, and transverse bars were considered as major parameters. Zuo and Darwin [6] took into account the effect of rib area of bars on the bond stress, and proposed to use $\sqrt[4]{f'_c}$ rather than $\sqrt{f'_c}$, which was adopted in the ACI 408R-03 [2] recommendations. Canbay and Frosch [7] applied split tension cracking failure to consider the effects of cover concrete and transverse bars on the bond strength. Issa and Assaad [8] reported that the bond strength decreases as the level of washout loss increases in underwater concrete, and proposed a regression model to predict the ultimate bond strength. Hwang et al. [9] proposed a non-uniform bond stress distribution model to predict the development length of tension bars, addressing the bar bond strength per unit length and the bond stress distribution along the development length, and the model was also applied to the development length of hooked bars [10], headed bars [11], and compression bars [12]. Assaad and Daou [13] investigated the effect of styrene-butadiene rubber latexex on the bond strength of concrete using recycled aggregates. Assaad and Issa [14] proposed regression statistical models to predict the combined effect of free water,

* Corresponding author.
E-mail addresses: hwanggun85@naver.com (H.-J. Hwang), baekja1@snu.ac.kr (J.-W. Baek), kimjyo@kw.ac.kr (J.-Y. Kim), changsookim@seoultech.ac.kr (C.-S. Kim).

https://doi.org/10.1016/j.engstruct.2019.109535
Received 29 May 2019; Received in revised form 8 August 2019; Accepted 10 August 2019
Available online 22 August 2019

Nomenclature

Notations

A_s	cross-sectional area of longitudinal bars (mm^2)
A_{tr}	total area of transverse bars (mm^2)
b	bias in the input and hidden layers
c	cover concrete in ACI 408R-03 (mm)
c_b	thickness of bottom cover concrete (mm)
c_{si}	one-half of center-to-center spacing of reinforcing bars (mm)
c_{so}	thickness of side cover concrete (mm)
d	normalized target value
d_b	bar diameter (mm)
f'_c	concrete compressive strength (MPa)
f_n	bond strength increment (MPa)
f_p	predicted tensile stress of bar splice (MPa)
f_t	actual tensile stress of bar splice (MPa)
f_y	bar yield strength (MPa)
K_{tr}, K_{atr}, K, K_{mtr}	coefficient for arrangement of transverse bars in ACI 318-14, Eurocode 2, ACI 408R-03, and fib Model Code 2010, respectively.
K_c	proposed coefficient for cover concrete and transverse bars in the modified ACI 318-14 method
k	number of training data
k_d	coefficient for arrangement of transverse bars in Model Code 2010
ℓ_d	development length (mm)
ℓ_s	lap splice length (mm)
$m_{j,1}^{(2)}$	momentum to improve the stability of learning
n_s	number of bars spliced along the splitting plane
s_t	center-to-center spacing of transverse bars (mm)
w	coefficient for cover concrete in Eurocode 2
$w_{i,j}^{(1)}$	weight value that connects between the input value x_i and j^{th} node of the first hidden layer
$w_{j,1}^{(2)}$	weight value that connects between the output value $y_j^{(1)}$ of the j^{th} node at the first hidden layer and the node of the output layer
x	normalized input
y	normalized output
$y_j^{(1)}$	output value at the j^{th} node of the first hidden layer
$z_j^{(1)}$	input value at the j^{th} node of the first hidden layer
$z^{(2)}$	input value at the node of the output layer
α	the training ratio (0 to 1)
α_d	coefficient of bar diameter in Hwang et al. method
α_t	coefficient for transverse bar diameter in fib Model Code 2010
β	coefficient related to momentum training ratio (0 to 1)
λ	coefficient of lightweight concrete
η_2	coefficient for bar diameter in Eurocode 2
η_3	coefficient for bar diameter in fib Model Code 2010
η_4	coefficient for bar yield strength
τ_u	coefficient for cover concrete and transverse bars in Hwang et al. method
ϕ	safety factor for structural design
ψ_e	coefficient for epoxy-coated bars
ψ_s	coefficient for bar diameter
ψ_t	coefficient for reinforcement location

viscosity modifier, lightweight aggregate, and styrene-butadient rubber latexex on the bond strength in semi-lightweight self-consolidating concrete. Hwang et al. [15] applied strain-rate effect to consider the effect of impact loading on the bond strength. Huang et al. [16] proposed a stochastic damage model to consider the bond stress variation along the development length.

Table 1
Current design codes for tension development length.

Design Codes	Equations for Tension Development Length (in MPa and mm)
ACI 318-14 [1]*	$\ell_d = \frac{f_y d_b}{1.1\lambda\sqrt{f'_c}} \frac{\psi_t\psi_e\psi_s}{(c_f + K_{tr})/d_b} \geqslant 300$ mm
ACI 408R-03 [2]**	$(c_f + K_{tr})/d_b \leqslant 2.5$, $c_f = \min(c_b, c_{so}, c_{si}) + 0.5d_b$, $K_{tr} = 40A_{tr}/(s_t n_s)$ $\ell_d = \frac{(f_y / 4\sqrt{f'_c} - \phi 57.4w)(\psi_t\psi_e\psi_s)d_b}{\phi 1.83(cw + K_{atr})/d_b}$
Eurocode 2 [3]***	$(cw + K_{atr})/d_b \leqslant 4.0$, $w = 0.1(c_{max}/c_{min}) + 0.9 \leqslant 1.25$, $K_{atr} = 6\sqrt{f'_c}\, t_d A_{tr}/(s_t n_s)$, $t_d = 0.03d_b + 0.22$ $\ell_d = \alpha_2\alpha_3 \frac{f_y d_b}{4f_{bd}} \geqslant \frac{\ell_0}{1.5}$
fib Model Code 2010 [4]****	$\alpha_2 = 0.7 \leqslant 1 - 0.15(c_d - d_b)/d_b \leqslant 1.0$, $\alpha_3 = 0.7 \leqslant 1 - K(\Sigma A_{tr} - A_s)/A_s \leqslant 1.0$, $f_{bd} = 2.25\eta_2[0.7(0.3)(f'_c)^{2/3}]$ $\ell_d = \frac{f_y d_b}{4f_{mbd}} \geqslant \ell_{m0}$ $f_{mbd} = (\alpha_{m2} + \alpha_{m3})f_{bd0} < 2.5f_{bd0} < \sqrt{f'_c}$, $f_{bd0} = 0.35\eta_3\eta_4\sqrt{f'_c}$, $\alpha_{m2} = \sqrt{(c_d/d_b)}\,(c_m/c_d)^{0.15}$, $\alpha_{m3} = k_d(K_{mtr} - \alpha_t/50) \geqslant 0$, $K_{mtr} = \Sigma A_{tr}/(s_t n d_b) \leqslant 0.05$

* λ = lightweight factor (0.75 to 1.0); ψ_t = reinforcement location factor (1.0 to 1.3); ψ_e = coating factor (1.0 to 1.5); ψ_s = bar diameter factor (0.8 to 1.0); c_b = thickness of the bottom cover concrete; c_{so} = thickness of the side cover concrete; c_{si} = one-half of the center-to-center spacing of bars; A_{tr} = total area of confining reinforcement within spacing s_t across the potential splitting plane; n_s = number of bars being developed or lap spliced along the splitting plane; and s_t = center-to-center spacing of transverse bars. The confinement term $(c_f + K_{tr})/d_b$ is limited to 2.5 considering danger of pull-out failure. When lap splices are used, the required lap splice length ℓ_s is defined as $1.0\ell_d$ or $1.3\ell_d$ for the class A or B splice (when the total area of spliced bars is greater than two times the required and less than half of bars are spliced within the required lap splice length, class A, otherwise, class B).

** $c = c_{min} + d_b/2$; $c_{max} = \max(c_b, c_s)$; $c_{min} = \min(c_b, c_s)$; $c_s = \min(c_{so}, c_{si} + 6.4)$; and $\phi = 0.82$ = safety factor for structural design. In ACI 408R-03, $\ell_s = \ell_d$.

*** $\alpha_2\alpha_3 \geqslant 0.7$; $c_d = \min(c_b, c_{so}, c_{si})$; $\ell_0 = \max(0.45d_b f_y/4f_{bd}, 15d_b, 200\,mm)$; K = coefficient for arrangement of transverse bars (0 to 0.1); ΣA_{tr} = total cross-sectional area of transverse bars within the development length; A_s = maximum cross-sectional area of the bar; and $\eta_2 = (132 - d_b)/100$ = coefficient for bar diameter (≤ 1.0). In Eurocode 2, ℓ_s varies between $1.0\ell_d$ and $1.5\ell_d$ according to the area ratio of spliced bars within $0.65\ell_d$, and a partial safety factor is applied to concrete for structural design.

**** $\ell_{m0} = \max(0.7d_b f_y/4f_{bd}, 15d_b, 200\,mm)$; k_d = coefficient for arrangement of transverse bars (0 to 20); α_t = coefficient for transverse bar diameter (0.5 for D25 to 1.0 for D50); $c_m = \max(c_{so}, c_{si})$; $\eta_3 = (25/d_b)^{0.3}$ = coefficient for bar diameter (≤ 1.0); and η_4 = coefficient for bar yield strength (0.68 to 1.2). In fib Model Code 2010, ℓ_s varies between $0.7\ell_d$ and $1.0\ell_d$ according to the area ratio and tensile stress of spliced bars within the lap splice length, and a partial safety factor is applied to concrete for structural design.

Recently, machine learning (or deep learning) has been widely used in civil engineering [17–19]. With the advanced computer intelligence, it is possible to transform input data into a more abstract and composite representation. Golafshani et al. [20] applied artificial neural networks and fuzzy logic models to predict the bond strength of reinforcing bars in 179 splice test results. Mashrei et al. [21] used back-propagation neural network to predict the bond strength of FRP-to-concrete joints in 150 single-lap shear test results. Makni et al. [22] applied artificial neural networks to predict the bond strength in 117 pull-out test results. Yaseen et al. [23] used polynomial chaos expansions to predict the development length in 534 splice test results. With enough number of test data, machine learning can be used to identify patterns in the data or to find underlying relations among test parameters, which is advantageous to achieve better design. A large number of test results with various design parameters are now available in the literature for the development and lap splice length design. Thus, further research is required using the test results and machine learning.

In the present study, to improve design reliability and to extend design application range for the development and lap splice lengths, an artificial neural network model (ANN, a machine learning algorithm) is presented using existing experimental studies for splice tests (total 1008 splice specimens having contact splices of same size bars, splice length of ℓ_s = 50–2489.2 mm, bar diameter of d_b = 8.0–57.3 mm, bar yield strength of f_y = 269.1–1058.0 MPa, and concrete compressive strength of f'_c = 6.9–113.9 MPa). Although some of the test parameters are out of the limitations of design codes (e.g. $d_b \leqslant 35.8$ mm, $f_y \leqslant 420$ MPa, and $f'_c \leqslant 70$ MPa in ACI 318–14 [1] because of lack of adequate experimental data), all test results were used for the ANN to extend design application range considering present-day construction materials and practices. From a parametric study, the effect of design variables was investigated, and predictions by the ANN were compared with existing design equations. Finally based on the parametric study result, modifications were proposed for existing design equations to consider the effect of non-uniform bond stress distribution and the effect of cover concrete and transverse bars, as well as to extend design application range.

2. Existing design equations for tension development length

To determine major explanatory variables for the input layer of the ANN, existing design equations were reviewed first. As summarized in Table 1, current design codes (ACI 318-14 [1], ACI 408R-03 [2], Eurocode 2 [3], and fib Model Code 2010 [4]) define the required tension development length ℓ_d as a function of the bar diameter d_b, bar yield strength f_y, and concrete compressive strength f'_c (in the table, some of notations differ from the original, which were replaced for direct comparison and consistency among all the codes). Additionally, the effect of split tension cracking is included by considering the cover concrete thickness and spacing of bars (Fig. 1). Current design codes define the required lap splice length ℓ_s based on the required development length ℓ_d and lap splice conditions: $\ell_s = 1.0\ell_d$ or $1.3\ell_d$ in ACI 318-14 [1], $1.0\ell_d$ in ACI 408R-03 [2], between $1.0\ell_d$ and $1.5\ell_d$ in Eurocode 2 [3], or between $0.7\ell_d$ and $1.0\ell_d$ in fib Model Code 2010 [4] (Table 1).

Meanwhile, Hwang et al. [9] proposed Eq. (1) for the tension development length.

$$\ell_d = \frac{f_y d_b}{\phi 3.26 \tau_u} \tag{1a}$$

$$\tau_u = 0.91\alpha_d \sqrt{f'_c}\left[\frac{(cw + K_{atr})/d_b}{2.5}\right] \tag{1b}$$

where ϕ= safety factor for structural design (=0.7); α_d = 1.1 for D19 bars or smaller, 1.0 between D22 and D29 bars, and 0.9 for D32 bars or greater; and c, w, and K_{atr} are defined in the same manner as ACI 408R-03 [2] (Table 1). In the equation, the lap splice length ℓ_s is defined as $\ell_s = \ell_d$, and relatively simple pullout test results are also applicable to the equation.

Input variables for learning of the ANN were selected from the existing design equations: the development length ℓ_d; bar diameter d_b; bar yield strength f_y; concrete compressive strength f'_c; effective area of confining reinforcement $A_{tr}/(n_s s_t d_b)$ (A_{tr} = total area of transverse bars, n_s = number of bars being developed or lap-spliced, and s_t = center-to-center spacing of transverse bars); bottom concrete cover-to-bar diameter ratio c_b/d_b (c_b = thickness of bottom cover concrete); side concrete cover-to-bar diameter ratio c_{so}/d_b (c_{so} = thickness of side cover concrete); and spliced bar spacing-to-bar diameter ratio c_{si}/d_b (c_{si} = one-half of spacing of spliced bars).

3. Artificial neural networks

3.1. Model composition

Fig. 2 shows the artificial neural networks, which consists of an input layer, a hidden layer, and an output layer. For simplicity, only one hidden layer was used. The input layer receives the values of the selected input variables, and each node of the input layer is connected to nodes of the hidden layer. As a constant value, a bias (b) was included in the input layer (also in the hidden layer). The values entering a hidden node were determined after multiplying the input and bias by weights ($w_{i,j}$) as follows.

$$z_j^{(1)} = \sum_{i=1}^{n+1} w_{i,j}^{(1)} x_i \tag{2}$$

where $z_j^{(1)}$ = input value at the j - th node of the hidden layer; $w_{i,j}^{(1)}$ = weight between the i - th input node and the j - th hidden node; i = location of an input node (1 to $n+1$ including a bias node); j = location of a hidden node (1 to m); n = total number of the selected input variables; and m = total number of hidden nodes except a bias node. It is noted that the value of each input node was normalized to be between −1 and 1, $w_{n+1,j}^{(1)} = b_j^{(1)}$ and $x_{n+1} = 1$ to consider the bias in the input layer, and the values of weight ($w_{i,j}^{(1)}$) and bias ($b_j^{(1)}$) were randomly initialized to be between −1 and 1 at the initial step and then updated by training.

A tangent-sigmoid function was used for the activation function in the hidden layer to transform $z_j^{(1)}$ into $y_j^{(1)}$.

$$y_j^{(1)} = f_1(z_j^{(1)}) = \frac{2}{1 + \exp(-2z_j^{(1)})} - 1 \tag{3}$$

where $y_j^{(1)}$ = output value at the j - th hidden node, which is between −1 and 1.

The output values of hidden modes and a bias (b) are concentrated on a node of the output layer.

$$z^{(2)} = \sum_{j=1}^{m+1} w_{j,1}^{(2)} y_j^{(1)} \tag{4}$$

where $z^{(2)}$ = input value at the node of the output layer; and $w_{j,1}^{(2)}$ = weight between the j - th hidden node and the output node. It is noted that $y_{m+1}^{(1)} = 1$ and $w_{m+1,1}^{(2)} = b_1^{(2)}$ to consider the bias in the hidden layer, and the values of weight ($w_{j,1}^{(2)}$) and bias ($b_1^{(2)}$) were randomly

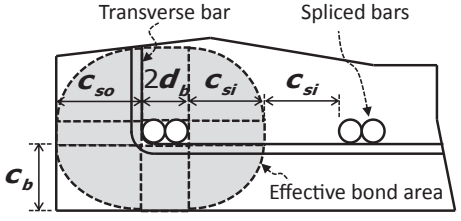

Fig. 1. Effect of cover concrete on bond strength.

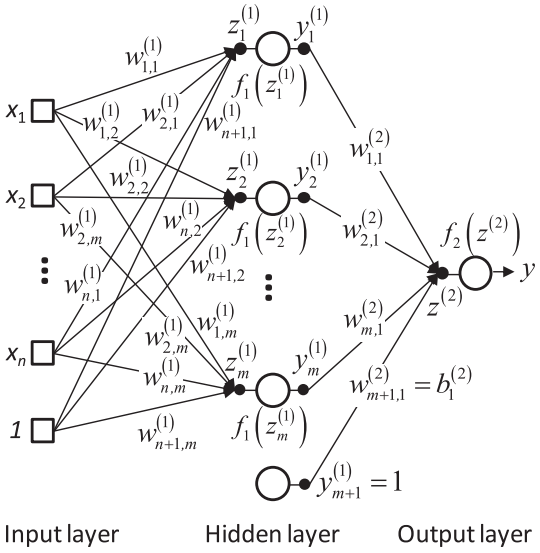

Fig. 2. Artificial neural networks with a hidden layer.

initialized to be between −1 and 1 at the initial step and then updated by training.

In the output layer, a linear activation function was used to determine the final output value (y).

$$y = f_2(z^{(2)}) = z^{(2)} \tag{5}$$

3.2. Back propagation

Fig. 3 shows the back propagation for updating the weight and bias in each layer. On the basis of the back propagation algorithm [24], the weight $w_{j,1}^{(2)}$ between the hidden and output layers can be updated by the weight increment $\Delta w_{j,1}^{(2)}$, which is calculated from the output value $y_j^{(1)}$ at the j - th hidden node and the difference between the actual output (or final output value, y) and expected output (or normalized target value, d) for learning. It is noted that $j = 1$ to $m + 1$ are used to update $w_{m+1,1}^{(2)}$ for the bias.

$$e = d - y \tag{6a}$$

$$\delta = f_2'(z^{(2)})e = e \tag{6b}$$

$$\Delta w_{j,1}^{(2)} = \alpha \delta y_j^{(1)} = \alpha y_j^{(1)}(d - y) \tag{6c}$$

$$[m_{j,1}^{(2)}]_k = [\Delta w_{j,1}^{(2)}]_k + \beta [m_{j,1}^{(2)}]_{k-1} \tag{6d}$$

$$[w_{j,1}^{(2)}]_{k+1} = [w_{j,1}^{(2)}]_k + [m_{j,1}^{(2)}]_k \tag{6e}$$

where $e =$ error; $\alpha =$ training ratio (0 to 1); $\beta =$ coefficient related to momentum training ratio (0 to 1); $k =$ number of training data; and $[m_{j,1}^{(2)}]_0 =$ initial momentum to improve the stability of learning (set as 0).

In the same manner, the weight $w_{i,j}^{(1)}$ between the input and hidden layers can be updated as follows.

$$e_j^{(1)} = w_{j,1}^{(2)} \times \delta = w_{j,1}^{(2)}(d - y) \tag{7a}$$

$$\delta_j^{(1)} = f_1'(z_j^{(1)}) \times e_j^{(1)} = (1 + f_1(z_j^{(1)}))(1 - f_1(z_j^{(1)}))e_j^{(1)} = (1 + y_j^{(1)})(1 - y_j^{(1)})e_j^{(1)} \tag{7b}$$

$$\Delta w_{i,j}^{(1)} = \alpha \delta_j^{(1)} x_i \tag{7c}$$

$$[m_{i,j}^{(1)}]_k = [\Delta w_{i,j}^{(1)}]_k + \beta [m_{i,j}^{(1)}]_{k-1} \tag{7d}$$

$$[w_{i,j}^{(1)}]_{k+1} = [w_{i,j}^{(1)}]_k + [m_{i,j}^{(1)}]_k \tag{7e}$$

where $[m_{j,1}^{(1)}]_0 =$ initial momentum to improve the stability of learning (set as 0); and $j = 1$ to m are used to update $w_{i,j}^{(1)}$.

All weights in Eqs. (2)–(7) were updated by using the training data. The calculations should be iterated until the accuracy converges into a target level or cannot be improved above a certain level. Thereafter, the ANN with the fixed values of weight can be used for prediction through Eqs. (2)–(5). It is noted that since Eq. (5) estimates the normalized y between −1 and 1, inverse normalization is necessary based on the normalized d for final prediction. Detailed descriptions are given in the next section.

3.3. Application

As stated before, design equations have limitations on their application because of lack of adequate experimental data. However, to extend design application range considering present-day construction materials and practices, the ANN was applied to 1008 existing splice tests for contact splices of same size bars [6,25–49], some of whose parameters are beyond the limitations of current design codes: test parameters were in the range of $\ell_s =$ 50–2489.2 mm for the lap splice length, $d_b =$ 8.0–57.3 mm for the bar diameter, $\ell_s/d_b =$ 5.0–82.5 for the splice length-to-bar diameter ratio, $f_y =$ 269.1–1058.0 MPa for the bar yield strength, $f_c' =$ 6.9–113.9 MPa for the compressive strength of concrete cylinder, $c_b/d_b =$ 0.2–7.0 for the bottom concrete cover-to-bar diameter ratio, $c_{so}/d_b =$ 0.1–12.8 for the side concrete cover-to-bar diameter ratio, $c_{si}/d_b =$ 0.2–12.8 for the spliced bar spacing-to-bar diameter ratio, $A_{tr}/(n_s s_t d_b) =$ 0–0.23 for the effective area of confining reinforcement, and $f_t =$ 129.5–1041.1 MPa for the actual tensile stress of lap splices (test results) (all summarized in Appendix A (Table A1)). Because current design provisions were established based on the bar tensile stress in a given splice length of the splice tests, the bar tensile stress was predicted using the ANN. Then, the ANN was trained by comparing the predicted and measured bar tensile stresses.

The following variables were used in the input layer (9 input nodes including a bias node of 1) on the basis of existing design equations [1–4,8]. In the ANN, the development length of $\ell_d = \ell_s$ was used.

$$[x_i]_{i=1\sim n+1} = \left[\ell_d \quad d_b \quad f_c' \quad f_y \quad \frac{A_{tr}}{n_s s_t d_b} \quad \frac{c_b}{d_b} \quad \frac{c_{so}}{d_b} \quad \frac{c_{si}}{d_b} \quad 1\right] \tag{8}$$

For data learning, the variables were normalized as follows, and put into Eq. (8).

$$x_i = \frac{2(x_i - x_{i,\min})}{x_{i,\max} - x_{i,\min}} - 1 \tag{9}$$

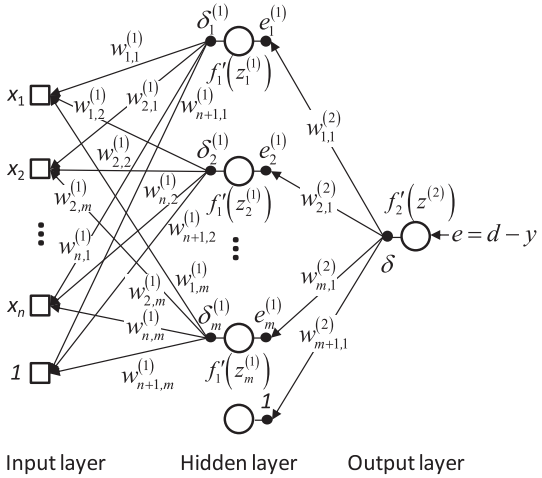

Fig. 3. Back propagation in artificial neural networks with a hidden layer.

where $x_{i,\min}$ and $x_{i,\max}$ = minimum and maximum values of a variable at the i - th input node, respectively. Using Eq. (9), the normalized target value (d) can be calculated from the test results f_t.

After data learning, the predicted tensile stress f_p of bar splices was calculated from the final output value y.

$$f_p = \frac{(y+1)(f_{t,\max} - f_{t,\min})}{2} + f_{t,\min} \tag{10}$$

where $f_{t,\min}$ and $f_{t,\max}$ = minimum and maximum values of actual tensile stress of bar splices.

Of the 1008 specimens, 80% (806 specimens) were used for training and the remaining 20% (202 specimens) were used for verification. In the training, total 20 hidden nodes were used (i.e., $m + 1 = 20$), α was varied between 0.1 and 0.001 according to an error level in the both of training and verification, and $\beta = 0.1$ was used. Strain hardening of reinforcing bars was neglected in learning according to existing design codes [1–4] (i.e., the maximum value of f_t was limited to the yield strength f_y of reinforcing bars). Eqs. (11a) and (11b) are the final weight matrices $w_{i,j}^{(1)}$ and $w_{j,1}^{(2)}$ for the input and hidden layers, respectively, after performing about 10000-step trainings, and these matrix-typed models for input variables can be used for practical application.

$$[w_{i,j}^{(1)}] = \begin{bmatrix}
-0.33 & 0.29 & 0.01 & -0.13 & 2.05 & 0.84 & -1.07 & 0.08 & 1.90 \\
-1.16 & 1.04 & -0.40 & 0.80 & -1.94 & -0.61 & -0.66 & 0.28 & -2.85 \\
0.05 & 0.61 & 0.61 & 0.49 & 0.39 & -0.05 & -1.20 & -0.07 & 0.33 \\
-0.65 & -0.72 & 0.39 & 0.25 & -0.81 & 0.75 & -0.70 & 1.17 & -0.87 \\
-0.13 & -0.40 & -0.46 & -1.65 & -1.97 & 0.38 & 0.76 & -0.36 & 0.15 \\
-0.21 & -1.04 & 0.20 & 0.56 & 0.73 & 0.28 & 0.49 & -2.17 & -0.69 \\
-0.35 & 2.62 & 0.34 & 1.43 & -0.44 & -0.33 & 1.44 & 0.52 & 0.92 \\
0.09 & -0.65 & -2.64 & -1.16 & -0.43 & 1.40 & 1.43 & 0.70 & 0.04 \\
1.50 & -0.14 & -0.46 & -0.76 & -0.52 & -0.04 & -0.16 & -0.15 & -0.47 \\
-2.26 & 0.46 & -1.30 & 1.22 & 1.50 & -0.06 & 0.78 & -1.49 & -2.36 \\
-1.19 & 1.56 & -0.98 & 0.86 & 0.09 & -0.19 & 0.10 & -0.94 & -0.02 \\
-2.25 & -1.56 & 0.33 & -1.12 & 0.81 & 0.57 & 0.29 & 0.09 & -1.83 \\
-1.73 & 0.18 & 0.12 & 1.15 & 1.36 & -0.36 & 0.80 & -1.83 & -0.02 \\
1.33 & -0.85 & 0.67 & -0.63 & -0.15 & 0.18 & -0.09 & -0.74 & -0.89 \\
-2.85 & -1.80 & 0.70 & -0.42 & 0.54 & 1.04 & -0.34 & 1.02 & -1.49 \\
-0.17 & 0.71 & 4.04 & 1.10 & 0.40 & -1.29 & -1.47 & -1.32 & -0.01 \\
-0.22 & -0.47 & 0.81 & -0.37 & 1.77 & 0.52 & 0.86 & 0.39 & 2.37 \\
0.58 & -2.35 & -0.61 & -0.29 & -0.15 & 0.61 & -1.14 & -0.75 & -0.87 \\
-0.16 & -0.13 & -0.28 & -1.11 & 2.93 & 0.69 & -0.48 & 0.01 & 2.26 \\
0.14 & -1.35 & -0.07 & 0.59 & -0.42 & 0.01 & 0.12 & 0.23 & 0.22
\end{bmatrix} \tag{11a}$$

$$[w_{j,1}^{(2)}(1{:}11)] = [1.87 \ \ -2.00 \ \ -2.25 \ \ -1.76 \ \ -1.61 \ \ 1.21 \ \ 0.88 \ \ -1.54 \ \ -2.66 \ \ -1.89 \ \ -1.59]^T$$
$$[w_{j,1}^{(2)}(12{:}21)] = [-1.40 \ \ -1.44 \ \ -1.64 \ \ 1.10 \ \ -0.96 \ \ -1.76 \ \ 1.33 \ \ -1.50 \ \ -1.84 \ \ -1.98]^T \tag{11b}$$

4. Parametric study

4.1. Comparison between test results and predictions

For comparison, the existing test results were compared with predictions by existing design equations and the ANN. Fig. 4 shows the test-to-prediction ratio f_t/f_p in terms of the lap splice length-to-diameter ratio ℓ_s/d_b. In the calculation of f_p, the basic development length was defined as $\ell_d = \ell_s/1.3$ for ACI 318-14 [1] and $\ell_d = \ell_s/1.5$ for Eurocode 2 [3] based on the actual conditions of each test specimen (for the other design equations, $\ell_d = \ell_s$), and safety factors were not considered for direct comparison. It is noted that a safety factor is implicitly included in ACI 318-14 [1]. In the figure, filled and hollow circles indicate the specimens with and without transverse bars, respectively.

As shown in the figure, ACI 318-14 [1], Eurocode 2 [3], and fib Model Code 2010 [4] underestimated the tensile stress of bar splices, especially in the range of $\ell_s/d_b \leqslant 40$, which is widely used in practice, and f_t/f_p tended to decrease as ℓ_s/d_b increased in those design codes. This is because those design codes assume uniform bond stress distribution neglecting local bond failure that is possible to occur when embedment length is relatively long. On the other hand, ACI 408R-03 [2] (mean and COV. of f_t/f_p = 1.01 and 0.169, where COV. = coefficient of variation) and the Hwang et al. method [9] (1.13 and 0.236) showed better predictions. As expected, the ANN showed the best prediction (1.02 and 0.100).

4.2. Parametric study

The high accuracy of the ANN could result from overfitting of machine learning to the given set of training data (i.e., the ANN could be too dependent on the training data, which is likely to have a higher error on new unseen data). To detect the overfitting and to investigate the effect of variables on the tensile stress of bar splices, a parametric study was performed by changing one variable and keeping the rest fixed. For validity of the parametric study results, the predictions were compared with the test results of 22 groups, which were carefully selected from the existing experimental studies (Table 2). Each group has only one variable, including the lap splice length-to-bar diameter ratio, bar diameter, bar yield strength, concrete compressive strength, cover concrete, and transverse bars.

Fig. 5 shows the parametric study results. In the figure, filled and hollow circles indicate the test results of two groups, and thin and thick lines indicate the predictions for the two groups, respectively. For

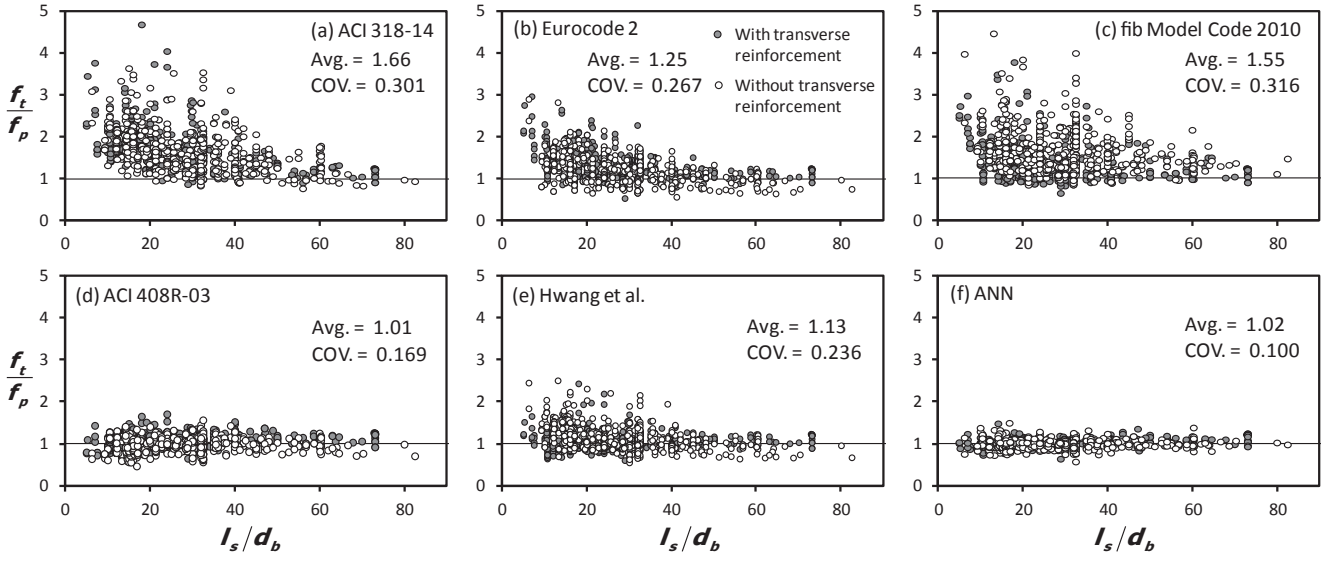

Fig. 4. Comparison of existing tests and predictions (without safety factors).

comparison, the prediction of ACI 408R-03 [2] showing the best accuracy among the existing design equations is also presented. As shown in the figure, the prediction of the ANN agreed well with the test results, showing a similar trend to that of ACI 408R-03 [2]. The tensile stress f_t of bar splices increased with the lap splice length-to-bar diameter ratio ℓ_s/d_b (Fig. 5(a)). Unexpectedly, f_t increased slightly in the case of using high-strength bars (Fig. 5(b)), which is in disagreement with the design codes: bond strength decreases as bar yield strength f_y increases (fib Model Code 2010 [4]) or it is not affected by f_y (ACI 408R-03 [2]: in the figure, f_p was limited to f_y for ACI 408R-03 [2]). On the other hand, the bar diameter d_b had no significant effect on f_t in the case of d_b larger than 20 mm (Fig. 5(c)). As the concrete strength f_c' increased, f_t increased (Fig. 5(d)). Without transverse bars, f_t tended to increase with the increase of the bottom concrete cover-to-bar diameter ratio c_b/d_b, side concrete cover-to-bar diameter ratio c_{so}/d_b, and spliced bar spacing-to-bar diameter ratio c_{si}/d_b (Fig. 5(e)–(g)), whereas with transverse bars, those effects were reduced (Fig. 5(h)–(j)). The effective area $A_{tr}/(n_s s_t d_b)$ of confining reinforcement also had an effect on f_t, but the increase of f_t with the increase of $A_{tr}/(n_s s_t d_b)$ was not significant when a sufficient concrete cover was provided (Fig. 5(k)).

5. Modification of existing design equations

For practical application of the advanced computer intelligence to design, modifications were proposed for two existing design equations: (1) ACI 318-14 [1] (Table 1), which is the simplest, and (2) the previously proposed method by Hwang et al. [9] (Eq. (1)). Keeping the original form of those equations, a factor related to local bond damage was newly introduced and an existing factor related to confinement was revised in the modification.

Generally in the current design equations, uniform bond stress distribution is assumed, which may not be exact particularly when embedment length is relatively long. Further, the design equations consider the effects of cover concrete and transverse bars (highly influential to the bond stress or splitting failure) in different ways. To consider these effects in design, two factors were derived, based on a large number of data obtained from existing experimental studies and learning of the ANN.

By fixing all other factors to be unity, the equation of ACI 318-14 [1] (Table 1) can be simplified as follows.

$$f_p = 1.1\sqrt{f_c'}\frac{\ell_d}{d_b} \tag{12}$$

As shown in Fig. 6(a), Eq. (12) underestimated the tensile stress of bar splices particularly for small ℓ_s/d_b, which was mainly attributed to uniform bond stress. When the embedment length is relatively short, bond stress along the bar can be assumed to be uniform using the unit bond stress of a local bond stress-slip relationship. However, when the embedment length is relatively long, the actual bond stress is not uniform and local bond damage occurs at the end of the bar, which decreases the bond stress locally. To simplify the effect of non-uniform bond stress distribution, a factor of f_n was assumed as a function of concrete strength on the basis of test results: 1) in a form of square root (Eq. (13a)); or 2) in a form of four square root (Eq. (13b)) as used in ACI 408R-03 [2].

$$f_p = 1.1\sqrt{f_c'}\frac{\ell_d}{d_b} + f_n = 1.1\sqrt{f_c'}\frac{\ell_d}{d_b} + 20\sqrt{f_c'} \tag{13a}$$

$$f_p = 1.1\sqrt{f_c'}\frac{\ell_d}{d_b} + f_n = 1.1\sqrt{f_c'}\frac{\ell_d}{d_b} + 50\sqrt[4]{f_c'} \tag{13b}$$

As compared in Fig. 6(b) and (c), Eq. (13b) showed better predictions. Thus, learning of the ANN was newly performed based on Eq. (13b). In the output layer, the target value (d) was normalized from the ratio of f_t/f_p.

Meanwhile, the effective bond area has an effect on splitting failure, and it is affected by the bottom concrete cover c_b, side concrete cover c_{so}, and spliced bar spacing c_{si} (Fig. 1), and a quarter of the elliptical area in Fig. 1 is related to two out of the three variables (c_b, c_{so}, and c_{si}). Thus, three combinations of $\sqrt{c_b c_{so}}$, $\sqrt{c_b c_{si}}$, and $\sqrt{c_{si} c_{so}}$ were used for variables in the input layer assuming that they are independent. The effective area $A_{tr}/(n_s s_t d_b)$ of confining reinforcement was also included (Eq. (14)) in the input layer. It is noted that the yield strength of transverse bars was not included due to its negligible effect [1-4,9].

$$[x_i]_{i=1\sim n+1} = \left[\frac{\sqrt{c_b c_{so}}}{d_b} \quad \frac{\sqrt{c_b c_{si}}}{d_b} \quad \frac{\sqrt{c_{si} c_{so}}}{d_b} \quad \frac{A_{tr}}{n_s s_t d_b} \quad 1\right] \tag{14}$$

Fig. 7 compares the test results and predictions by the newly modeled ANN (mean and COV. of f_t/f_p = 1.00 and 0.150). For the effect of cover concrete and transverse bars, a factor of K_c was included as given in the left side of Eq. (15), and K_c can be estimated by using the test results and predictions of the ANN.

$$1.1\sqrt{f_c'}\frac{\ell_d}{d_b}K_c + 50\sqrt[4]{f_c'} \approx \left(1.1\sqrt{f_c'}\frac{\ell_d}{d_b} + 50\sqrt[4]{f_c'}\right)\frac{f_t}{f_p} \tag{15}$$

The factor of K_c obtained from the learning is as given in Eq. (16).

$$K_c = 1.2 + \frac{\sqrt{c_b c_{so}} + \sqrt{c_b c_{si}} + \sqrt{c_{si} c_{so}}}{7d_b} + 7\sqrt{\frac{A_{tr}}{n_s s_t d_b}} \leqslant 4 \tag{16}$$

The modified ACI 318-14 method using the proposed K_c is given in Eq. (17). In the equation, two factors ψ_t and ψ_s for the reinforcement location and bar diameter were included according to ACI 318-14 [1] (Table 1), but the lightweight factor λ and coating factor ψ_e were not included because their effects were excluded in the database (Table A1). The development length ℓ_d of a reinforcing bar can be defined using $f_p = f_y$ in Eq. (17a).

$$f_p = 1.1\sqrt{f_c'}\frac{\ell_d}{d_b}\frac{K_c}{\psi_t\psi_s} + 50\sqrt[4]{f_c'} \leqslant f_y \tag{17a}$$

$$\ell_d = \frac{(f_y - 50\sqrt[4]{f_c'})d_b}{1.1\sqrt{f_c'}}\frac{\psi_t\psi_s}{K_c} \tag{17b}$$

Table 2
Existing test groups for parametric study.

Groups	Authors	Specimens
G1	Mathey and Watstein [28]	8-7-1; 8-14-1; 8-14-2; 8-21-2; 8-28-2; 8-34-1; 8-34-2
G2	Ferguson and Krishnaswamy [32]	SP33 + + +; SP34
G3	Kadoriku [42]	PB-19; PB-20
G4	Kadoriku [42]	PB-13; PB-24
G5	Hegger and Burkhardt [33]	B 2; B 8
G6	Ferguson and Krishnaswamy [32]	14S1; 18S12
G7	Hwang et al. [33]	40L3009S1; 55L3009S2; 55L3009S1; 70L3009S1
G8	Azizinamini et al. [39]	BB-11-5-36; BT-11-5-36; BB-11-15-36; BT-11-15-36
G9	Chinn et al. [25]	D23; D28
G10	Ferguson and Thompson [29]	C1; C9
G11	Darwin et al. [44]	6.3; 8.4
G12	Zuo and Darwin [6,47]	41.1-B-S-U; 42.1-B-S-U; 43.2-B-S-U
G13	Thompson et al. [34]	14-60-4/2/2-5/5; 14-60-4/2/4-5/5
G14	Thompson et al. [34]	11-30-4/2/2-6/6; 11-30-4/2/4-6/6
G15	Stöckl et al. [33]	I3; II5; II9; III13; IV21
G16	Stöckl et al. [33]	II14; IV17; IV18
G17	Eligehausen [33]	S60A1; S60A2; S60A3; S120A1; S120A2; S120A3
G18	Chamberlin [27]	3a; 3b; 3c
G19	Stöckl et al. [33]	I1; IV22
G20	Darwin et al. [44]	7.5; 8.2; 9.3
G21	Hester et al. [40]	8C5-16-0-U; 8C5-16-2-U; 8C5-16-4-U
G22	Tepfers [33]	657-9; 657-10

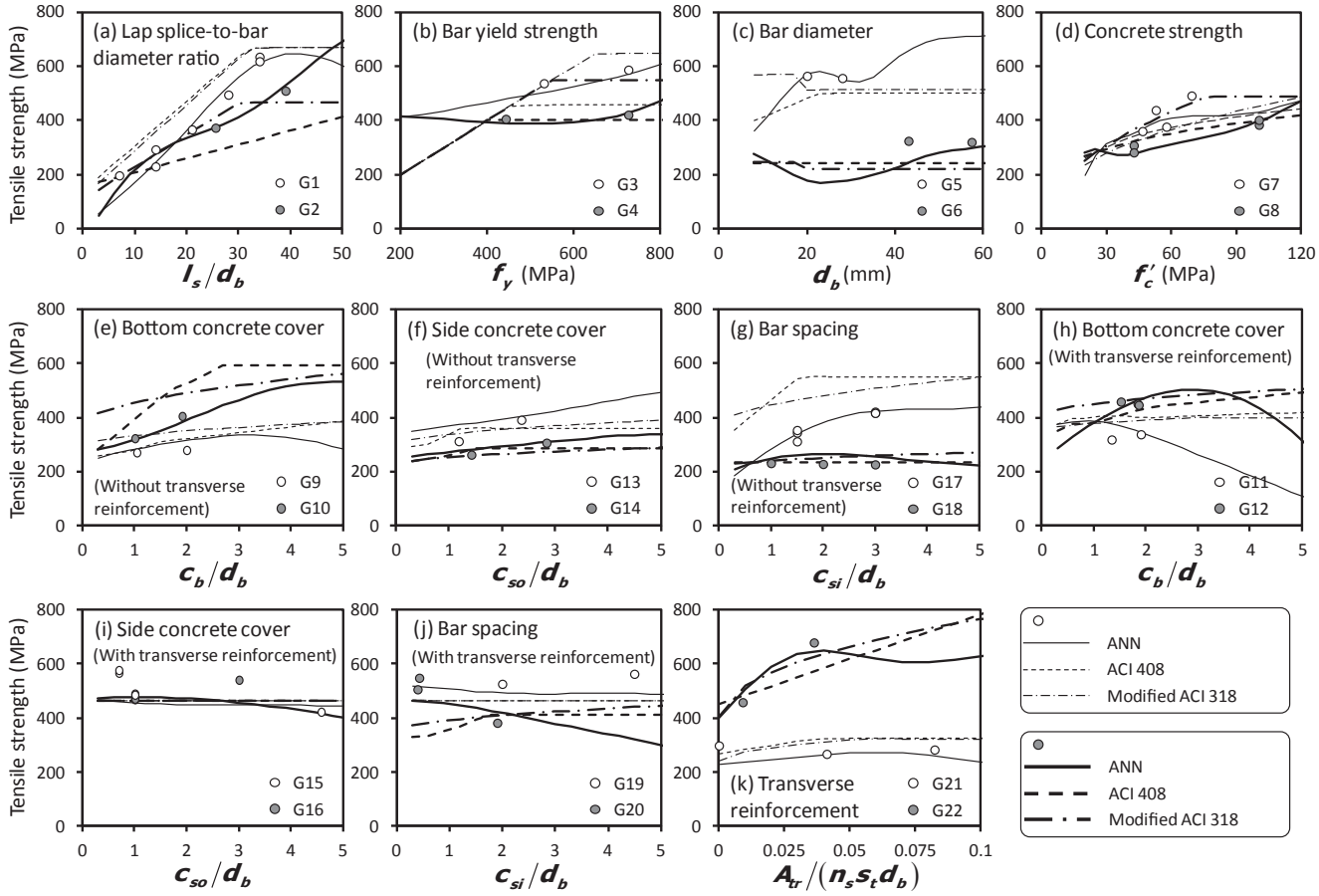

Fig. 5. Parametric study results.

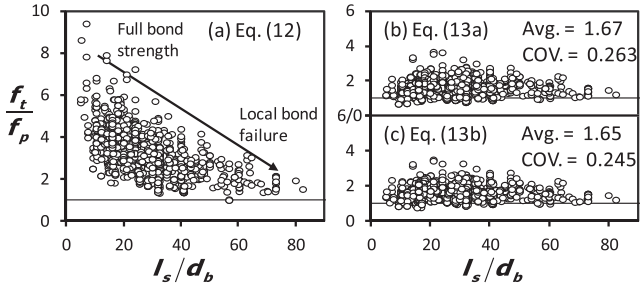

Fig. 6. Simplified effect of non-uniform bond stress distribution on bond strength.

In a similar manner, the equation of Hwang et al. [9] was also modified as given in Eq. (18), using the proposed K_c.

$$f_s = 2.5\tau_u \frac{l_d}{d_b} + 50\sqrt[4]{f'_c} \leqslant f_y \tag{18a}$$

$$\ell_d = \frac{f_y - 50\sqrt[4]{f'_c}}{2.5\tau_u} d_b \tag{18b}$$

$$\tau_u = 0.91\alpha_d \sqrt{f'_c}\left(\frac{K_c}{2.5}\right) \tag{18c}$$

As shown in Fig. 8 when compared to Fig. 4(d) and (e), the modifications improved the accuracy of the design equations: the mean and COV. of f_t/f_p were improved from 1.66 and 0.301 to 1.00 and 0.152 for ACI 318-14 [1] ($\ell_d = \ell_s/1.3$), or from 1.13 and 0.236 to 0.99 and 0.156 for the Hwang et al. method [9] ($\ell_d = \ell_s$).

For design purpose, a safety factor needs to be included in the design equations. For a 5% fractile (quantile) with 90% confidence level (z-score $z_p = 1.645$) [50], the maximum ratio of unsafe design (unconservative prediction) should be less than 5% (50 of the 1008 test specimens), and this corresponded to a safety factor of approximately $\phi = 0.85$ (Eq. (18)) in the ANN: mean $- z_p \times$ SD ≈ 0.85, where mean $=$ 1.02 and SD $=$ standard deviation $=$ COV.$\times$mean $=$ 0.102 for the ANN.

$$f_t = 0.85f(y) \leqslant f_y \tag{19}$$

For conservative prediction, the design equations of the modified ACI 318-14 method (Eq. (20)) and the modified Hwang et al. method (Eq. (21)) can be defined as follows.

$$\ell_d = \frac{(f_y - 34\sqrt[4]{f'_c})}{0.75\sqrt{f'_c}} d_b \frac{\psi_t \psi_s}{K_c} \geqslant 300 \text{ mm} \tag{20}$$

$$\ell_d = \frac{f_y - 34\sqrt[4]{f'_c}}{1.7\tau_u} d_b \tag{21}$$

Fig. 9 compares the test results and predictions by the design equations including the safety factor. It is noted that the partial safety factor of concrete was applied for Eurocode 2 [3] (i.e., $f_{bd}/1.5$) and fib Model Code 2010 [4] (i.e., $f_{bd0}/1.5$) (see Table 1). As shown in the figure, the modified ACI 318–14 method and the modified Hwang et al. method showed better predictions than the original ACI 318–14 and Hwang et al. methods, satisfying the target design safety. For the modified ACI 318-14 method, the mean and COV. of f_t/f_p were 1.39 and 0.183, and the unsafe design ratio was 4.6% (46 of the 1008 test specimens). For the modified Hwang et al. method, the mean and COV. were 1.37 and 0.184, and the unsafe design ratio was 4.8% (48 of the 1008 test specimens).

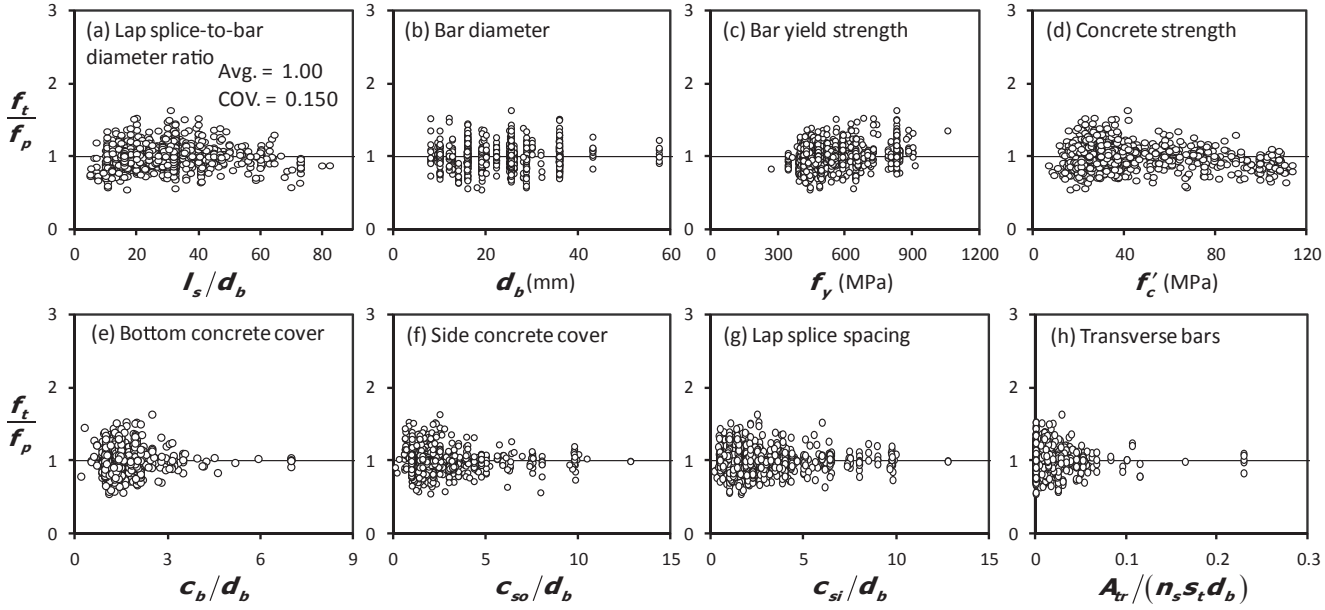

Fig. 7. Predictions by ANN with simplified design parameters.

6. Summary and conclusions

In the present study, to improve design reliability and to extend design application range for the development and lap splice lengths, an artificial neural network model (ANN) was presented using 1008 existing specimens for splice tests. Although some of the test parameters are out of the limitations of design codes, all test results were used for the ANN to extend design application range considering present-day construction materials and practices. The major research findings are summarized as follows.

1) Based on existing design equations, eight primary design parameters (i.e., the bar development length, bar diameter, bar yield strength, concrete compressive strength, bottom concrete cover, side concrete cover, spliced bar spacing, and effective area of confining reinforcement) were selected as variables for the input nodes of the ANN. Using the existing test results, the ANN was trained and verified, and then the final weight matrices $w_{i,j}^{(1)}$ and $w_{j,1}^{(2)}$ for the input and hidden layers were provided.
2) The predictions by the existing design equations and the ANN were compared with the existing test results. ACI 318-14, Eurocode 2, and fib Model Code 2010 underestimated the tensile stress of bar splices, which resulted mainly from non-uniform bond stress distribution and splitting failure. On the other hand, ACI 408R-03 and the Hwang et al. method showed better predictions, and the ANN showed the best prediction.
3) To detect the overfitting and to investigate the effects of the input variables, a parametric study was performed using a single variable. The parametric study showed that learning of the ANN was significantly dependent on the given set of training data, and some of the input variables had limited effects on the tensile stress of bar splices.
4) Based on the parametric study result, modifications were proposed for ACI 318-14 and the Hwang et al. method to consider the effect of non-uniform bond stress distribution (or bond stress distribution along the undamaged length) and the effect of concrete cover and transverse bars on splitting failure, as well as to extend design application range. Comparisons showed that the modifications improved the accuracy of the design methods: the mean and COV. of test-to-prediction ratios were 1.00 and 0.152 for the modified ACI 318-14 method or 0.99 and 0.156 for the modified Hwang et al. method, respectively. For design purpose, the modified design equations were proposed to satisfy that unsafe design ratio was less than 5%. The high accuracy to the large number of existing test results confirms that the modifications based on the ANN can improve design reliability and also can extend design application range for the development and lap splice lengths.

It is noted that this research focused on the bond performance of straight bars in tension as the beginning of the study in an attempt to apply ANN to development and lap splice length design. In order to apply ANN to development and lap splice length design of straight bars in compression, hooked bars in tension, and headed bars, further research is required.

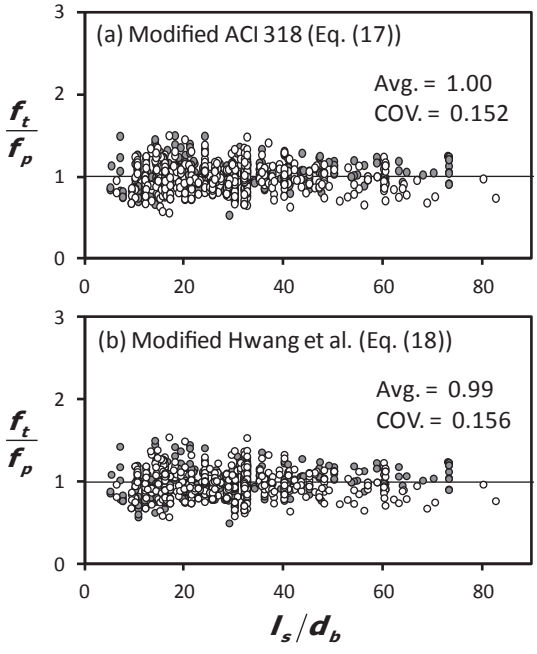

Fig. 8. Comparison of existing tests and proposed methods.

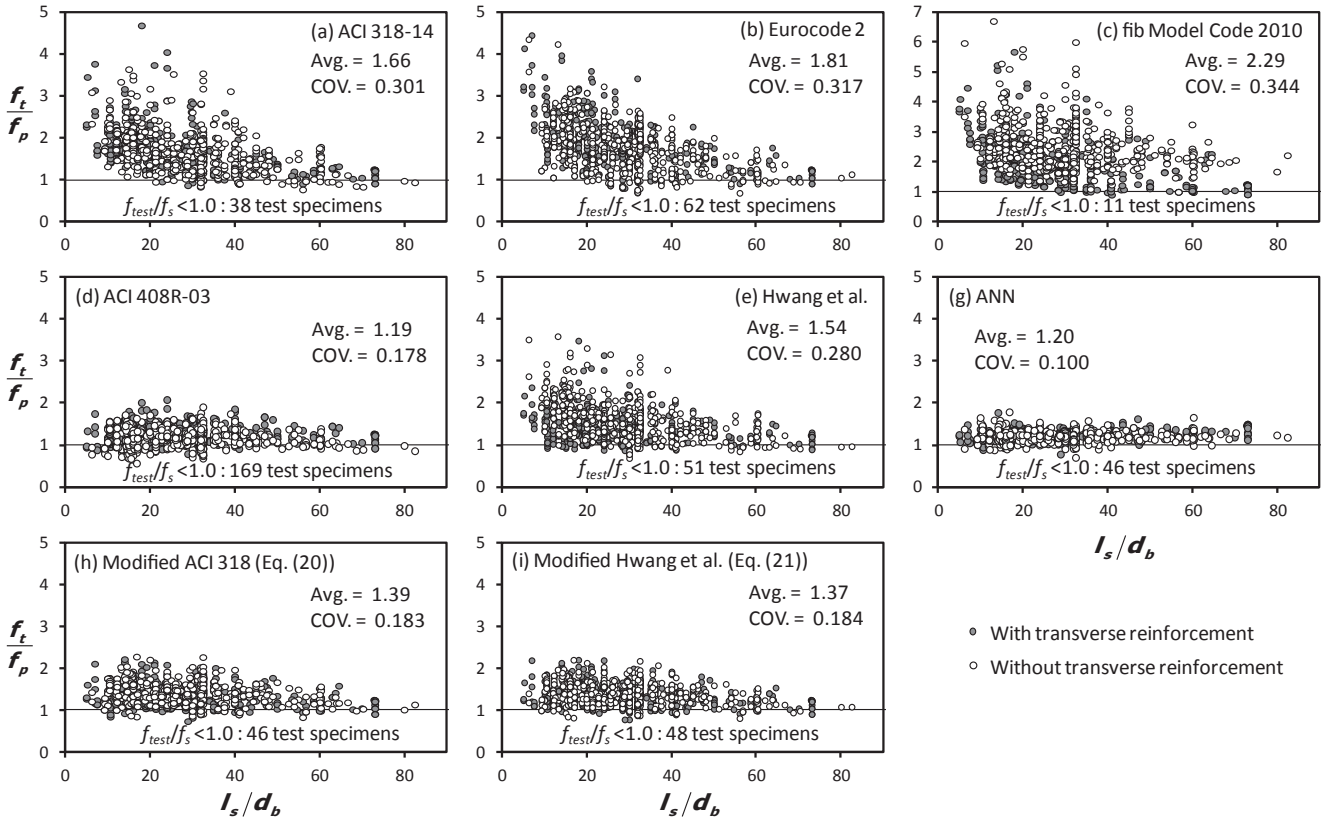

Fig. 9. Comparison of existing tests and predictions (with safety factors).

Declaration of Competing Interest

The authors declare that there are no known conflicts of interest.

Acknowledgement

This research was financially supported by the National Natural Science Foundation of China (Grant No. 51851110760) and the Research Program funded by the SeoulTech (Seoul National University of Science and Technology). The authors are grateful to the authority for the supports.

Appendix A. Test parameters of existing experimental studies

Table A1 summarizes the major test parameters of 1008 splice test specimens obtained from existing experimental studies [6,25–49].

Table A1
Test parameters of existing bar-splice test specimens.

Specimens	Number of tests	l_s (mm)	d_b (mm)	f_c' (MPa)	f_y (MPa)	c_b/d_b	c_{so}/d_b	c_{si}/d_b	$100A_{tr}/(n_s s_t d_b)$	f_t (MPa)
Chinn et al. [25]	39	139.7	9.5	21.8	393.3	0.82	1.00	0.50	0.00	164.8
		609.6	35.8	51.6	545.1	2.26	3.93	3.93	2.20	416.4
Chamberlin [26]	11	152.4	12.7	25.4	400.0	1.33	1.00	1.00	0.00	238.2
		406.4	19.1	40.5	400.0	2.00	3.00	9.00	0.00	340.3
Chamberlin [27]	12	152.4	12.7	30.2	345.0	2.00	1.00	1.00	0.00	226.2
		304.8	12.7	32.0	345.0	2.00	5.00	5.00	0.00	352.5
Mathey and Watstein [28]	14	177.8	12.7	24.1	669.3	1.50	3.50	2.50	9.52	197.3
		863.6	25.4	30.9	791.4	3.50	7.50	6.50	22.86	793.5
Ferguson and Thompson [29]	42	190.0	9.5	16.4	565.8	0.89	5.89	5.89	0.00	322.9
		1718.4	35.8	41.1	603.8	4.52	12.79	12.79	0.00	630.7
Ferguson and Breen [30]	35	457.2	25.4	12.6	434.7	0.93	1.42	1.43	0.00	285.1
		2148.0	35.8	38.8	683.1	1.75	3.26	3.35	1.93	665.2
Ferguson and Briceno [31]	32	812.8	25.4	16.9	448.5	1.42	0.58	0.55	0.00	276.0
		2159.0	35.8	30.0	483.0	2.00	3.03	3.03	0.98	531.3
Ferguson and Krishnaswamy [32]	22	381.0	15.9	18.1	269.1	0.53	1.00	0.99	0.00	263.0
		2489.2	57.3	32.1	503.7	1.42	8.01	8.01	3.26	510.0
Tepfers [33]	163	50.0	8.0	6.9	402.2	0.20	0.10	0.18	0.00	129.5
		1320.0	19.0	97.6	1058.0	5.94	10.44	6.19	0.00	793.6
Thompson et al. [34]	25	304.8	19.1	17.4	384.3	0.71	1.18	1.18	0.00	254.6
		1524.0	43.0	32.5	464.4	3.00	4.00	2.66	2.73	409.2

(*continued on next page*)

Table A1 (*continued*)

Specimens	Number of tests	l_s (mm)	d_b (mm)	f_c' (MPa)	f_y (MPa)	c_b/d_b	c_{so}/d_b	c_{si}/d_b	$100A_{tr}/(n_s s_t d_b)$	f_t (MPa)
Rehm, Eligehausen [33]	19	210.0	14.0	19.1	404.0	0.96	1.00	1.00	0.48	252.0
		1140.0	28.0	55.0	561.0	1.29	6.14	6.15	3.42	555.0
Stöckl, Menne, Kupfer [33]	24	780.0	18.0	17.2	444.0	0.62	0.69	1.00	0.95	338.0
		1900.0	26.0	29.2	465.0	1.28	6.50	8.00	2.43	576.0
Eligehausen [33]	8	299.0	12.0	27.8	550.0	2.00	2.00	1.50	0.00	311.4
		612.0	20.0	31.2	550.0	7.00	2.00	4.00	0.00	441.0
Betzle [33]	5	420.0	16.0	20.2	420.0	1.79	1.00	1.00	0.79	400.0
		1900.0	28.0	23.8	450.0	3.21	5.00	5.00	2.34	470.0
Zekany et al. [35]	24	406.4	28.7	25.5	414.7	1.42	1.42	1.26	0.00	218.9
		558.8	35.8	39.3	433.3	1.77	1.77	1.42	0.36	395.8
Olsen [33]	21	80.0	16.0	25.9	647.0	1.63	1.63	2.63	1.47	227.2
		480.0	16.0	83.9	647.0	1.63	1.63	2.63	4.42	714.0
Choi et al. [36]	10	304.8	15.9	37.0	435.4	1.33	1.42	1.42	0.00	214.5
		609.6	35.8	41.5	489.2	1.60	3.19	3.19	0.00	441.6
DeVries et al. [37]	20	228.6	19.1	51.5	458.2	0.94	1.16	1.16	1.63	214.2
		711.2	28.7	111.1	528.8	1.67	2.83	3.25	4.91	485.7
Rezansoffet al. [38]	34	384.0	19.5	22.2	420.2	0.71	1.01	1.19	1.08	307.4
		965.0	35.7	39.6	500.2	1.63	1.70	3.88	6.15	541.6
Azizinamini et al. [39]	18	330.2	25.4	35.1	488.5	0.98	0.98	1.29	0.00	192.5
		2032.0	35.8	104.3	537.2	1.00	1.00	1.50	0.00	490.6
Hester et al. [40]	32	254.0	19.1	34.7	440.0	1.83	2.00	1.50	0.00	248.4
		578.0	25.4	44.5	499.0	3.14	4.35	4.32	16.41	472.0
Rezansoffet al. [41]	15	300.0	25.2	25.0	445.0	1.71	1.55	0.49	0.00	235.0
		1125.0	29.9	28.2	475.0	2.02	1.84	1.00	5.67	527.2
Kadoriku [42]	34	380.0	19.0	21.2	442.3	1.50	1.53	2.94	1.58	300.1
		950.0	19.0	75.8	843.4	3.50	4.74	6.42	3.84	807.0
Hwang et al. [33]	18	150.0	28.7	46.6	478.0	1.00	1.00	1.00	0.00	277.0
		300.0	28.7	84.0	518.6	1.74	1.74	1.48	4.94	492.1
Azizinamini et al. [43]	10	1016.0	35.8	75.2	488.5	1.13	1.13	1.13	0.00	323.6
		2032.0	35.8	113.9	508.7	1.13	1.13	1.13	1.04	552.7
Darwin et al. [44]	66	254.0	15.9	26.4	414.0	1.22	1.05	0.40	0.00	305.9
		1016.0	35.8	36.2	558.9	2.94	3.35	5.10	6.67	557.0
Hamad and Itani [45]	8	305.0	25.0	52.3	426.3	1.52	1.52	1.60	0.00	266.8
		305.0	25.0	76.8	426.3	1.52	1.52	1.60	0.00	391.2
Hegger and Burkhardt [33]	9	300.0	20.0	80.0	557.0	1.00	1.00	1.00	0.00	510.0
		850.0	28.0	100.0	591.0	2.00	2.00	1.00	5.34	591.0
Azizinamini et al. [46]	70	254.0	25.4	35.1	488.5	0.98	0.98	1.00	0.00	192.5
		2032.0	35.8	113.9	537.2	2.13	2.13	2.26	3.67	556.6
Zuo and Darwin [6,47]	98	406.4	15.9	29.3	434.6	1.03	1.39	0.39	0.00	353.5
		1016.0	35.8	108.0	555.9	3.06	4.03	3.86	5.17	575.1
Seliem et al. [48]	58	381.0	15.9	28.0	830.0	1.12	1.25	1.38	0.00	468.9
		2311.4	35.8	70.3	830.0	3.19	6.07	6.01	2.84	1041.1
Choi et al. [49]	12	373.0	12.7	24.7	650.0	1.26	1.57	2.52	0.00	549.0
		1700.0	31.8	55.3	720.0	3.15	3.15	4.65	1.86	720.0

*l_s: splice length; d_b: bar diameter; f_c': concrete compressive strength; f_y: bar yield strength; c_b: bottom concrete cover; c_{so}: side concrete cover; c_{si}: one-half of the center-to-center spacing of reinforcing bars; A_{tr}: total cross-sectional area of transverse bars within spacing s_t; n_s: number of spliced bars; s_t: center-to-center spacing of transverse bars; f_t: test result; and the top and bottom values indicate the minimum and maximum values, respectively.

References

[1] ACI Committee 318, Building Code Requirements for Structural Concrete and Commentary, American Concrete Institute, Farmington Hills, MI, 2014, 519 pp.
[2] ACI Committee 408, Bond and Development of Straight Reinforcing Bars in Tension (ACI 408R-03), American Concrete Institute, Farmington Hills, MI, 2003, 49 pp.
[3] British Standards, Eurocode 2: Design of Concrete Structures, BS EN 1992-1:2004, 2004, 225 pp.
[4] fib, fib Model Code for Concrete Structures 2010, fib, Ernst & Sohn, Germany, 2010, 420 pp.
[5] Orangun CO, Jirsa JO, Breen JE. A reevaluation of test data on development length and splices. ACI J, Proc 1977;74(3):114–22.
[6] Zuo J, Darwin D. Splice Strength of conventional and high relative rib area bars in normal and high-strength concrete. ACI Struct J 2000;97(4):630–41.
[7] Canbay E, Frosch RJ. Bond strength of lap-spliced bars. ACI Struct J 2005;102(4):605–14.
[8] Issa CA, Assaad JJ. Bond of tension bars in underwater concrete: effect of bar diameter and cover. Mater Struct 2015;48:3457–71.
[9] Hwang HJ, Park HG, Yi WJ. Nonuniform bond stress distribution model for evaluation of bar development length. ACI Struct J 2017;114(4):839–49.
[10] Hwang HJ, Park HG, Yi WJ. Development length of standard hooked bar based on non-uniform bond stress distribution. ACI Struct J 2017;114(6):1637–48.
[11] Hwang HJ, Park HG, Yi WJ. Development length of headed bar based on nonuniform bond stress distribution. ACI Struct J 2019;116(2):29–40.
[12] Hwang HJ, Park HG, Yi WJ. Development length of compression reinforcing bar based on nonuniform bond stress distribution. ACI Struct J 2018;115(6):1695–705.
[13] Assaad JJ, Daou Y. Behavior of structural polymer-modified concrete containing recycled aggregates. J Adhes Sci Technol 2017;31(8):874–96.
[14] Assaad JJ, Issa CA. Stability and bond properties of latex-modified semi-lightweight flowable concrete. ACI Mater J 2018;115(4):519–30.
[15] Hwang HJ, Zang L, Ma G. Effect of impact loading on bar development length in CCT node. J Struct Integrity Maint 2019;4(1):26–36.
[16] Huang L, Ye H, Chu S, Xu L, Chi Y. Stochastic damage model for bond stress-slip relationship of reinforcing bar embedded in concrete. Eng Struct 2019;194:11–25.
[17] Flood I, Kartam N. Neural networks in civil engineering. I: Principles and understanding. J Comput Civil Eng 1994;8(2):131–48.
[18] Adeli H. Neural networks in civil engineering: 1989–2000. Comput-Aided Civ Infrastruct Eng 2001;16(2):126–42.
[19] Lee S, Ha J, Zokhirova M, Moon H, Lee J. Background information of deep learning for structural engineering. Arch Comput Methods Eng 2018;25(1):121–9.
[20] Golafshani EM, Rahai A, Sebt MH, Akbarpour H. Prediction of bond strength of spliced steel bars in concrete using artificial neural network and fuzzy logic. Constr Build Mater 2012;36:411–8.
[21] Mashrei MA, Seracino R, Rahman MS. Application of artificial neural networks to predict the bond strength of FRP-to-concrete joints. Constr Build Mater 2013;40:812–21.
[22] Makni M, Daoud A, Karray MA, Lorrain M. Artificial neural network for the prediction of the steel-concrete bond behaviour. Eur J Environ Civil Eng 2014;18(8):862–81.

[23] Yaseen ZM, Keshtegar B, Hwang HJ, Nehdi ML. Predicting reinforcing bar development length using polynomial chaos expansions. Eng Struct 2019;195:524–35.
[24] Rumelhart DE, Hinton GE, Williams RJ. Learning Representations by Back-propagating errors. Nature 1986;323:533–6.
[25] Chinn J, Ferguson PM, Thompson JN. Lapped splices in reinforced concrete beams. ACI J, Proc 1955;52(2):201–13.
[26] Chamberlin SJ. Spacing of reinforcement in beams. ACI J, Proc 1956;53(1):113–34.
[27] Chamberlin SJ. Spacing of spliced bars in beams. ACI J, Proc 1958;54(8):689–98.
[28] Mathey R, Watstein D. Investigation of bond in beam and pull-out specimens with high-yield-strength deformed bars. ACI J, Proc 1961;32(9):1071–90.
[29] Ferguson PM, Thompson JN. Development length of high strength reinforcing bars in bond. ACI J, Proc 1962;59(7):887–922.
[30] Ferguson PM, Breen JE. Lapped splices for high-strength reinforcing bars. ACI J, Proc 1965;62(9):1063–78.
[31] Ferguson PM, Briceno A. Tensile Lap Splices-Part 1: Retaining Wall Type, Varying Moment Zone. Research Report No. 113-2, Center for Highway Research, The University of Texas at Austin, 1969.
[32] Ferguson PM, Krishnaswamy CN. Tensile Lap Splices-Part 2: Design Recommendation for Retaining Wall Splices and Large Bar Splices. Research Report No. 113-2, Center for Highway Research, The University of Texas at Austin, 1971, 60 pp.
[33] fib Task Group 4.5 “Bond models”, Splice test database May be obtained from http://fibtg45.dii.unile.it/files%20scaricabili/Database_splicetest%20Stuttgart%20sept%202005.xls; 2005.
[34] Thompson MA, Jirsa JO, Breen JE, Meinheit DF. The Behavior of Multiple Lap Splices in Wide Sections. Research Report No. 154-1, Center for Highway Research, The University of Texas at Austin, 1975, 75 pp.
[35] Zekany AJ, Neumann S, Jirsa JO, Breen JE. The Influence of Shear on Lapped Splices in Reinforced Concrete. Research Report No. 242-2, Center for Transportation Research, Bureau of Engineering Research, The University of Texas at Austin, 1981, 88 pp.
[36] Choi OC, Hadje-Ghaffari H, Darwin D, McCabe SL. Bond of epoxy-coated reinforcement: bar parameters. ACI Mater J 1991;88(2):207–17.
[37] DeVries RA, Moehle JP, Hester W. Lap Splice of Plain and Epoxy-Coated Reinforcements: An Experimental Study Considering Concrete Strength, Casting Position, and Anti-Bleeding Additives. Report No. UCB/SEMM-91/02 Structural Engineering Mechanics and Materials, University of California, Berkeley, California, 1991, 86 pp.
[38] Rezansoff T, Konkankar US, Fu YC. Confinement Limits for Tension Lap Splices under Static Loading. Report No. S7N 0W0, University of Saskatchewan, 1991.
[39] Azizinamini A, Stark M, Roller JJ, Ghosh SK. Bond performance of reinforcing bars embedded in high-strength concrete. ACI Struct J 1993;90(5):554–61.
[40] Hester CJ, Salamizavaregh S, Darwin D, McCabe SL. Bond of epoxy-coated reinforcement: splices. ACI Struct J 1993;90(1):89–102.
[41] Rezansoff T, Akanni A, Sparling B. Tensile lap splices under static loading: A review of the proposed ACI 318 code provisions. ACI Struct J 1993;90(4):374–84.
[42] Kadoriku J. Study on behavior of lap splices in high-strength reinforced concrete members. Doctorate Thesis, Kobe University, Japan, 1994, 201 pp.
[43] Azizinamini A, Chisala M, Ghosh SK. Tension development length of reinforcing bars embedded in high-strength concrete. Eng Struct 1995;17(7):512–22.
[44] Darwin D, Tholen ML, Idun EK, Zuo J. Splice strength of high relative Rib area reinforcing bars. ACI Struct J 1996;93(1):95–107.
[45] Hamad BS, Itani MS. Bond strength of reinforcement in high-performance concrete: The role of silica fume, casing position, and superplasticizer dosage. ACI Mater J 1998;95(5):499–511.
[46] Azizinamini A, Pavel R, Hatfield E, Ghosh SK. Behavior of spliced reinforcing bars embedded in high strength concrete. ACI Struct J 1999;96(5):826–35.
[47] Zuo J, Darwin D. Bond strength of high relative rib area reinforcing bars. SM Report No. 46, University of Kansas Center for Research, Lawrence, Kansas, 1998, 350 pp.
[48] Seliem HM, Hosny A, Rizkalla S, Zia P, Briggs M, Miller S, et al. Bond characteristics of ASTM A1035 steel reinforcing bars. ACI Struct J 2009;106(4):530–9.
[49] Choi WS, Park HG, Chung L, Kim JK. Experimental study for class B lap splice of 600 MPa(87 ksi) reinforcing bars. ACI Struct J 2014;111(1):49–58.
[50] Natrella MG. Experimental Statistics. National Bureau of Standards Handbook 91, United States Department of Commerce, 1966.